Miner Deposita (2017) 52:69–84
DOI 10.1007/s00126-016-0647-y

ARTICLE

Comparison of the native antimony-bearing Paiting gold deposit, Guizhou Province, China, with Carlin-type gold deposits, Nevada, USA

Zhuo-Jun Xie[1,2,3] · Yong Xia[1] · Jean S. Cline[3] · Bao-Wen Yan[4] · Ze-Peng Wang[5] · Qin-Ping Tan[6] · Dong-Tian Wei[1,2]

Received: 11 September 2015 / Accepted: 7 March 2016 / Published online: 15 March 2016

Abstract The Paiting gold deposit, Guizhou Province, China, has been regarded as a Carlin-type gold deposit by several researchers. Alteration and ore-related minerals from the Paiting deposit were examined, and results were compared with the Cortez Hills Carlin-type gold deposit, Nevada, USA. Similarities include the structural and stratigraphic controls on the orebodies in both deposits and the occurrence of invisible gold ionically bound in arsenian pyrite. Significant differences include the following: (1) The gold-bearing mineral in Nevada is arsenian pyrite. However, gold-bearing minerals in the Paiting deposit include arsenopyrite, arsenian pyrite, and trace pyrrhotite. Also, euhedral or subhedral gold-bearing arsenian pyrite at Paiting contains significantly less As, Cu, and Hg than gold-bearing pyrite from Nevada. (2) Alteration in the Paiting deposit displays significantly less decarbonatization. Instead, dolomite precipitation, which has not been described in Nevada deposits, is associated with deposition of gold-bearing sulfide minerals. (3) Stibnite and minor native antimony typify Paiting late-ore-stage minerals, whereas in Nevada, realgar, orpiment, and calcite are common late-ore-stage minerals. Precipitation of native antimony in the Paiting deposit reflects the evolution of a late-ore fluid with unusually low sulfur and oxygen fugacities. Some characteristics of the Paiting gold deposit, including formation of ore-stage dolomite and precipitation from CO_2-rich ore fluids at temperatures in excess of 250 °C, are more typical of orogenic deposits than Nevada Carlin deposits. The presence of similarities in the Paiting deposit to both Carlin type and orogenic deposits is consistent with formation conditions intermediate to those typical of Carlin type and orogenic systems.

Keywords Paiting gold deposit · Sediment-hosted gold deposit · Carlin-type deposit · Deposit comparison · Native antimony

Editorial handling: K. Kelley

Electronic supplementary material The online version of this article (doi:10.1007/s00126-016-0647-y) contains supplementary material, which is available to authorized users.

✉ Yong Xia
xiayong@vip.gyig.ac.cn

Zhuo-Jun Xie
chdxiezhuojun@126.com

[1] State Key Laboratory of Ore Deposit Geochemistry, Institute of Geochemistry, Chinese Academy of Sciences, Guiyang 550002, China

[2] University of Chinese Academy of Sciences, Beijing 100039, China

[3] University of Nevada Las Vegas, Las Vegas, Nevada 454010, USA

[4] Zijin Mining Group Northwest Co., LTD. Mining Geology Survey Institute, Urumqi 830026, China

[5] No. 105 Geological Party, Guizhou Bureau of Geology and Mineral Exploration and Development, Guiyang 550018, China

[6] Institute of Geophysical and Geochemical Exploration, Chinese Academy of Geological Sciences, Langfang 102849, China

Introduction

The sediment-hosted gold deposits in Guizhou Province, China (Fig. 1), have been described as geologically similar to the Carlin-type gold deposits in Nevada, USA (Gao et al. 2002; Hu et al. 2002; Li et al. 2002; Su et al. 2008, 2012; Xia et al. 2009; Chen et al. 2011), the second largest known concentration of gold in the world (Muntean et al. 2011). The Guizhou deposits are distributed along the southwestern margin of the Yangtze Craton (Hu et al. 2002; Fig. 1) and are primarily hosted by Late Paleozoic–Early Mesozoic

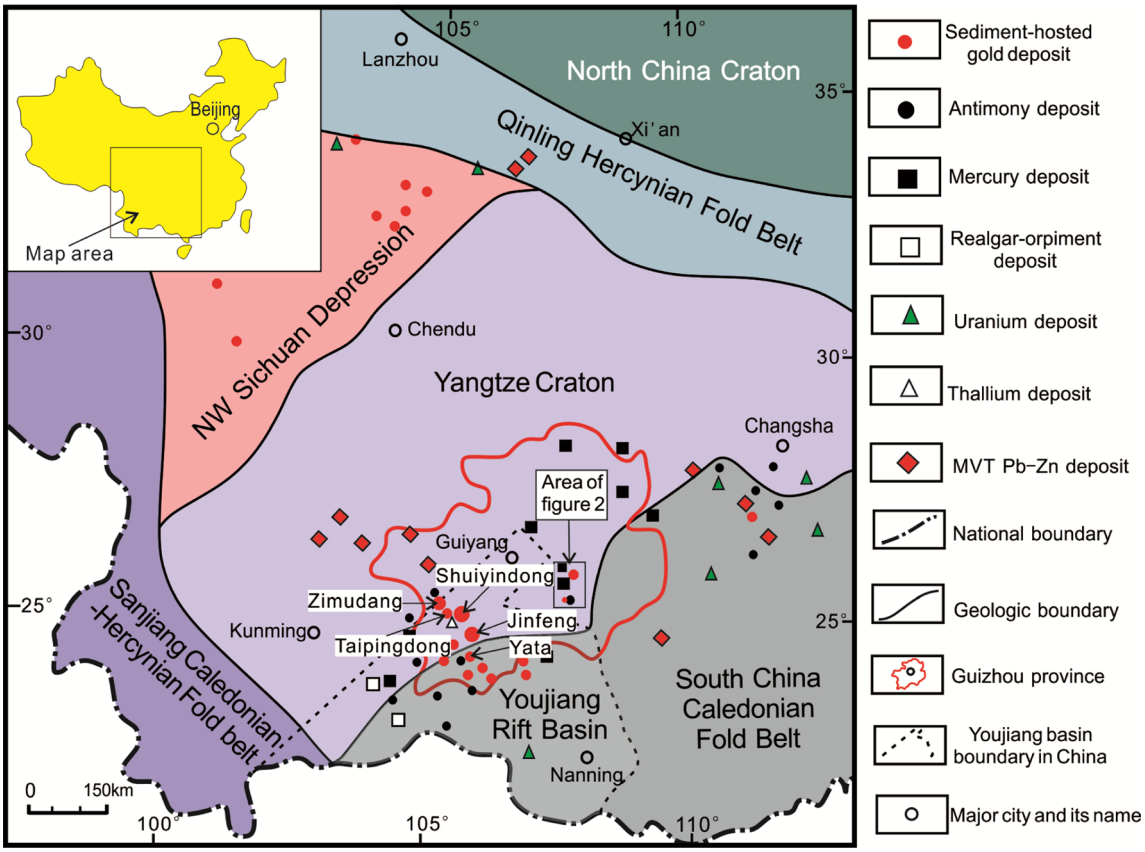

Fig. 1 Location map showing major cities, tectonic units, sediment-hosted gold deposits, and other epithermal ore deposits in Southwest China. Note that the majority of the sediment-hosted gold deposits are located in the southwestern Guizhou Province (*area inside red line*) (modified from Hu et al. 2002)

sedimentary rocks in southwestern Guizhou Province, with some deposits hosted by Early Paleozoic sedimentary rocks in southeastern Guizhou Province (Hu et al. 2002). Although the Guizhou sediment-hosted gold deposits are much smaller than the Nevada Carlin-type gold deposits, they exhibit many of the characteristics of the Nevada deposits. One of the significant similarities in these two districts is that the vast majority of Au is invisible as it substitutes for Fe in the pyrite structure (Simon et al. 1999; Palenik et al. 2004; Su et al. 2012). Another similarity is that the deposits in both areas are enriched in As, Sb, Hg, and Tl in addition to Au (Arehart 1996; Hu et al. 2002; Cline et al. 2013). These elements typically occur in Au-bearing pyrite and as sulfide minerals (e.g., realgar, orpiment, and stibnite) and rarely occur as native elements, except that trace native As has been found in both Nevada (Rytuba 1985) and Guizhou deposits (Zhuang et al. 1998; Tan 2001; Liu et al. 2007; Wang 2013).

Native antimony is a relatively rare mineral in nature, as it is only stable at low oxygen and sulfur fugacities (Normand et al. 1996; Williams-Jones and Normand 1997). To date, native antimony has only been reported in antimony or gold-antimony deposits (Normand et al. 1996; Bellot 2003; Thorne et al. 2008; An and Zhu 2010) or lead-zinc deposits (Li et al. 2005), and it has not been reported in Carlin-type gold deposits in Nevada, USA, or in sediment-hosted gold deposits in Guizhou Province, China, other than in the Paiting deposit.

This study compares the Paiting gold deposit with Carlin-type gold deposits in Nevada, with a focus on ore and alteration minerals in the Cortez Hills deposit, a Carlin-type gold deposit that exhibits characteristics typical of Nevada deposits. Our results show that the Paiting deposit not only exhibits some characteristics of the Nevada Carlin-type deposits, including sediment-hosted ore and invisible gold in arsenian pyrite, but also displays significant differences, including the morphology and chemistry of gold-bearing minerals and dolomite-stable alteration. Another important discovery in this study is that native antimony formed in the Paiting deposit during the late-ore stage. Based on the mineral assemblages that formed at the Paiting deposit during the ore and late-ore stages, the physicochemical conditions of native antimony and ore formation in the Paiting gold deposit have been constrained.

Geological background

Characteristics of classic Carlin-type gold deposits in Nevada, USA

Over 80–90 % of gold in Nevada Carlin-type gold deposits occurs in four areas, including the Carlin, Cortez and Getchell trends, and the Jerritt Canyon district (Cline et al. 2005). The characteristics of the deposits in these four districts are remarkably similar (Cline et al. 2005). Critical geologic characteristics that define the Nevada deposits were identified and include the following: (1) The deposits formed from ~42 to 34 Ma, corresponding to a change from compression to tension and renewed magmatism, resulting in a spatial and temporal relationship of the deposits with the proximal magmatic activity (Hofstra et al. 1999; Cline et al. 2005; Ressel and Henry 2006; Muntean et al. 2011). (2) Ore deposits occur in clusters or are aligned along old, reactivated basement rift structures. Orebodies exhibit both structural and stratigraphic controls, and the deposits are preferentially hosted by carbonate-bearing rocks within or adjacent to structures in the lower plate of a regional thrust (Cline et al. 2005; Muntean et al. 2011). (3) Ionically bound gold occurs within trace element-rich arsenian pyrite or marcasite that formed by sulfidation of host rock Fe (Hofstra et al. 1991; Arehart 1996; Simon et al. 1999; Cline et al. 2005; Reich et al. 2005). (4) Alteration processes associated with gold precipitation include decarbonatization that removed carbonate from the rock, silicification in the form of jasperoid replacement of carbonate minerals, and argillization of silty rock components to form illite and kaolinite (Cail and Cline 2001; Cline et al. 2005). (5) Orpiment, realgar, and lesser stibnite precipitated during the late-ore stage in open space as the system cooled and collapsed (Hofstra et al. 1991; Cline et al. 2005; Muntean et al. 2011). (6) Elements that characterize the Nevada Carlin-type deposits include Au, As, Hg, Tl, Cu (Te), and Sb, with low to absent Ag and base metals (Muntean et al. 2011). (7) The deposits generally formed at depths of less than ~3 km and at temperatures of 180–240 °C, from moderately acidic ($pH \leq 5$), reduced fluids containing <5 wt% NaCl equiv, <4 mol% CO_2, <0.4 mol% CH_4, and >0.01 mol% H_2S (Cline and Hofstra 2000; Hofstra and Cline 2000; Cline et al. 2005; Muntean et al. 2011; Lubben et al. 2012).

Geology of Cortez Hills Carlin-type gold deposit, Nevada

The Cortez Hills deposit, located on the Battle Mountain-Eureka trend, Nevada, is a high-grade Carlin-type gold deposit that exhibits typical characteristics of the Nevada Carlin-type gold deposits (Clark 2012; Clark et al., in review). The Cortez Hills deposit has proven gold reserves of 306 t with an average Au grade of 1.99 g/t (Barrick Gold Corp. 2014). The main host rocks are silty limestone and limestone of the Silurian Roberts Mountains, Devonian Wenban, and Devonian Horse Canyon formations (Arbonies et al. 2011; Jackson et al. 2011). Gold is hosted in arsenian pyrite that is encompassed by illlite and jasperoid (Clark 2012; Clark et al. in review). The host rock has been variably decarbonatized and silicified, and where decarbonatization was intense, a hydrothermal collapse breccia formed (Clark 2012; Clark et al. in review).

Geology of the Paiting gold deposit, Guizhou Province

The Sandu-Danzhai Hg-Au-Sb metallogenic belt in southeastern Guizhou Province contains a series of gold (Hg, Sb) deposits and occurrences, including the Paiting, Hongfachang, Xinfachang, Paihe, Yangyong, Miaolong, and Gaodong deposits (Fig. 2). These gold deposits, together with the gold deposits in Youjiang Basin (e.g., Shuiyindong and Jinfeng gold deposits, Fig. 1), have been described as geologically similar to the Carlin-type gold deposits in Nevada, USA (Gao et al. 2002; Hu et al. 2002; Li et al. 2002). The Paiting gold deposit is the largest gold deposit in the Sandu-Danzhai Hg-Au-Sb metallogenic belt (Dong 2007; Wu 2008), with proven reserves of 5 t and average gold grades of 4 g/t (Jiang Liu pers. commun. 2015).

The strata exposed in the Paiting deposit area consist of the pre-Sinian Xiajiang Group and Upper Sinian and Cambrian strata, which were deposited on the slope of the Qiannan platform margin (Wu 2008; Fan 2010) and are described by Wu (2008) (Figs. 3 and 4). Most rocks in the section are gray to black owing to the presence of abundant carbon (Wu 2008; Fan 2010). Gold mineralization preferentially occurs in limestone and mudstone of the Cambrian Bianmachong (∈1b), Wuxun (∈1w), and Duliujiang (∈2d) formations (Fig. 4). The Lower Cambrian Bianmachong Formation (∈1b) consists of black carbonaceous shale, with black silty mudstone at the base. The Lower Cambrian Wuxun Formation (∈1w) lies above the Bianmachong Formation and is subdivided into lower and upper units. The lower unit consists of gray to dark gray, sandy mudstone interbedded with carbonaceous mudstone, locally containing dolomitic nodules. The upper unit is dominated by light gray to dark gray mudstone and silty mudstone, interbedded with bedded limestone or muddy limestone. The Middle Cambrian Duliujiang Formation (∈2d) overlies the Wuxun Formation and is subdivided into lower, middle, and upper units. The lower unit, which is also cut by mineralized structures, consists of gray, sandy mudstone interbedded with mudstone at the base and mudstone interbedded with bedded muddy limestone at the top. The middle unit consists of chert at the base and dark gray, clastic dolomite, and bedded dolomite at the top. The upper unit is dominated by muddy dolomite, bedded limestone, and thick-bedded muddy limestone.

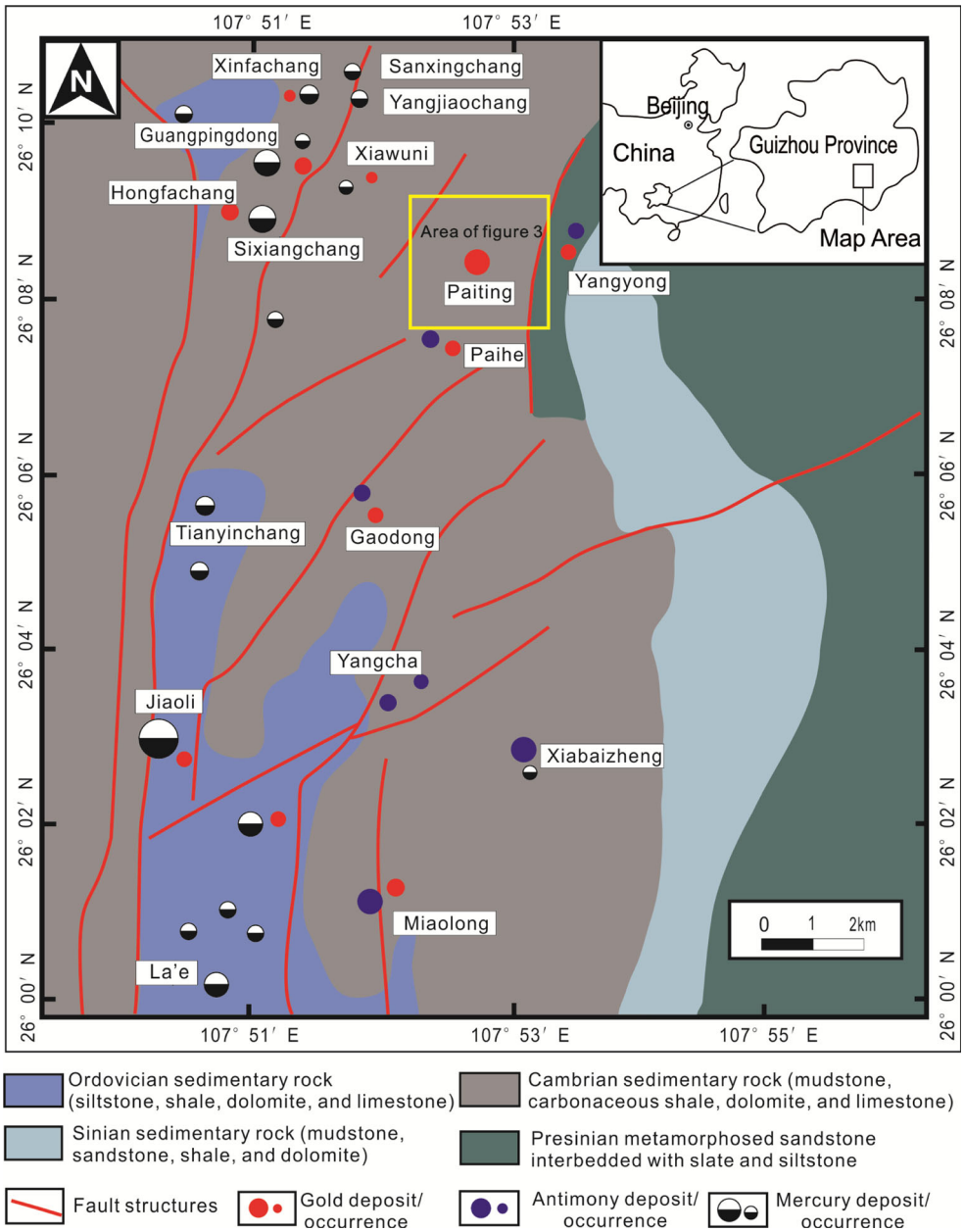

Fig. 2 Geological map of the Sandu-Danzhai Hg-Au-Sb metallogenic belt in Guizhou Province (modified from Gao et al. 2002)

Geologic mapping and drilling have yet to identify any igneous rocks in the Paiting district. Metamorphic rocks of Longli Formation (Ptxjl) (Figs. 3 and 4), including gray to gray-white, fine-grained to medium-grained metamorphosed sandstone interbedded with slate and siltstone, are exposed east of the Paiting deposit. Chemical analyses to date have not identified anomalous gold in these metamorphic rocks (Bureau of Non-ferrous Geological Exploration of Guizhou Province, unpublished report, 2010). The strata exposed in the Paiting gold deposit are part of a monocline (Fig. 3) that dips to the west from 15° to 50°. The Paiting district is characterized by complex faulting. These faults can be divided into ENE-, NE-, NNE-, and NW-striking faults. Most of the orebodies are hosted in the ENE- and NE-striking faults (Fig. 3).

In the Paiting gold deposit, submicron gold occurs in arsenopyrite and arsenian pyrite (Li et al. 2002). Commonly, these minerals are closely associated with jasperoid and illite, but are also associated with dolomite and calcite. Alteration associated with gold mineralization includes decarbonatization, silicification, dolomitization, sulfidation, and argillization (Gao et al. 2002; Li et al. 2002; Wu 2008; Fan 2010). Decarbonatization is characterized by the dissolution of calcite and ferroan dolomite. Silicification occurs as replacement of carbonate and formation of jasperoid, which contains abundant

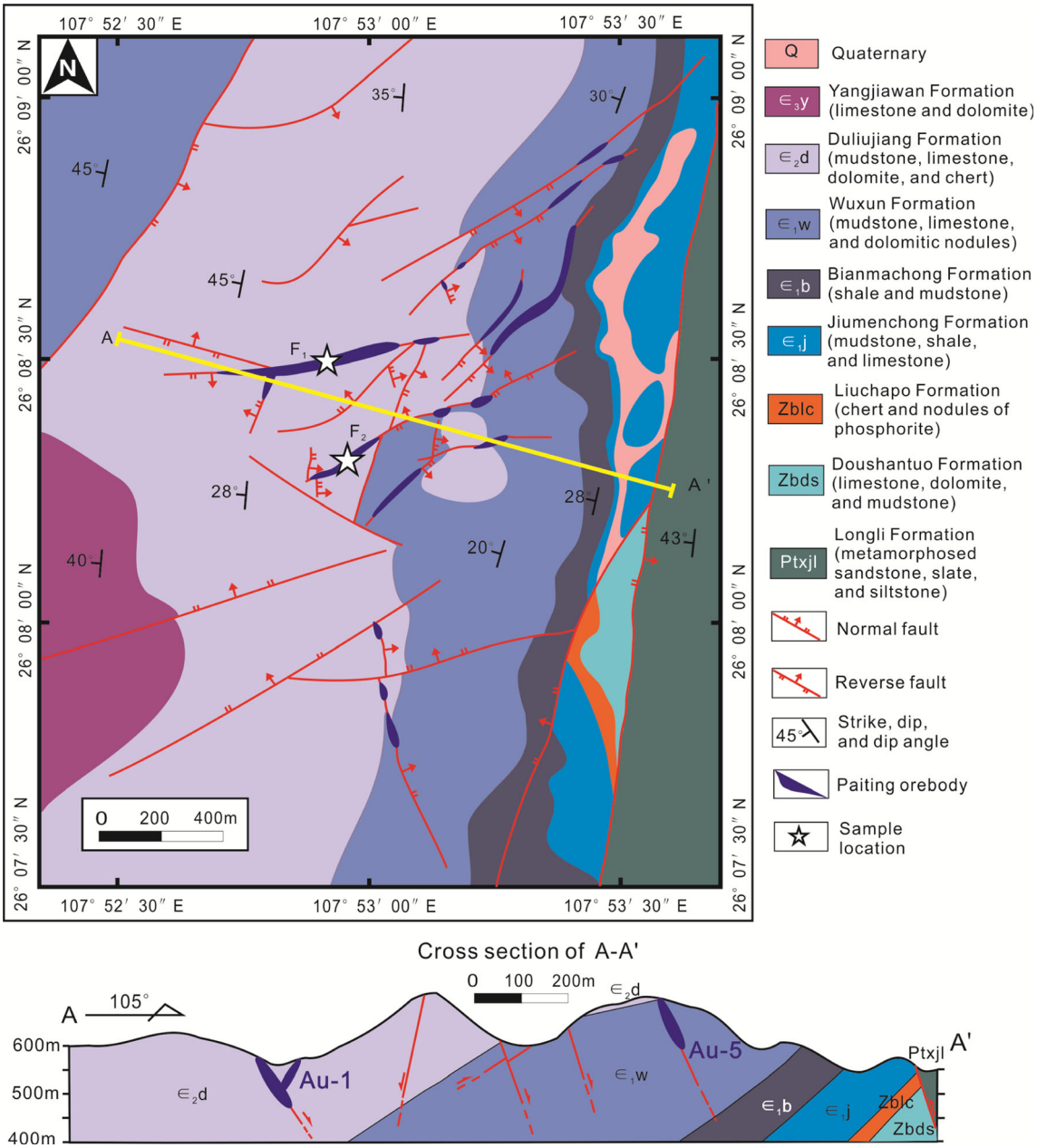

Fig. 3 Geological map of the Paiting gold deposit (modified from Bureau of Non-ferrous Geological Exploration of Guizhou Province, unpublished report 2010)

fine-grained calcite and ferroan dolomite inclusions. Wall rocks have been argillized by the formation of illite.

Methods

Seventy-one samples were collected from drill core and adits located along the main orebodies that are hosted by faults F_1 and F_2 in the Paiting deposit (Fig. 3). Eleven drill core samples, selected for examination of the Cortez Hills Carlin-type gold deposit, were chosen from a suite of samples previously collected from this deposit (Clark 2012). All samples were collected along short transects from low gold to high-grade rock. Forty-two polished sections were prepared and examined using transmitted and reflected light petrography, scanning electron microscopy (SEM), and electron probe microanalysis (EPMA).

A JEOL-5600 SEM at the University of Nevada Las Vegas (UNLV) Electron Microanalysis and Imaging Laboratory (EMiL) was used to provide semi-quantitative chemical compositions to confirm and identify minerals. High-resolution

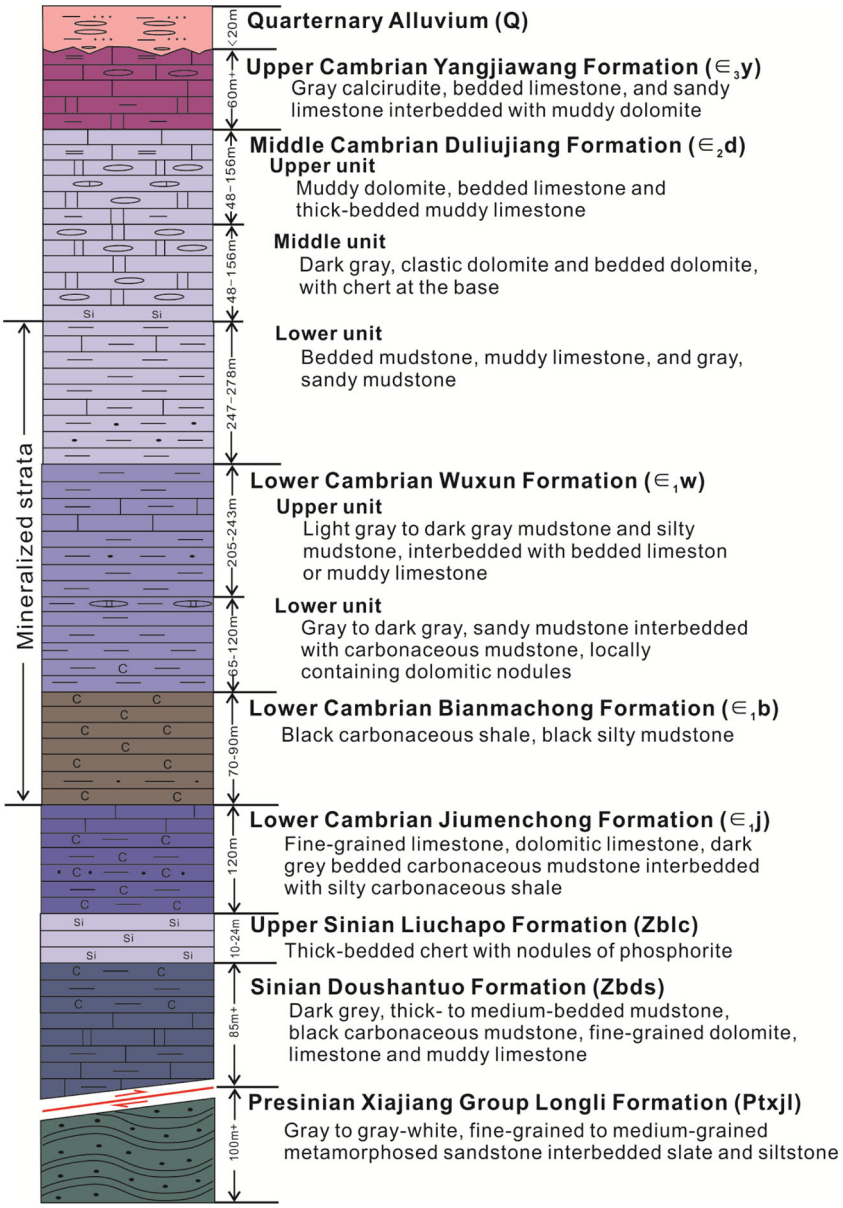

Fig. 4 Stratigraphic column for Paiting deposit, showing relationships between major orebodies and stratigraphy (Wu 2008; Bureau of Non-ferrous Geological Exploration of Guizhou Province, unpublished report 2010)

images were captured using the SEM to record textural and spatial relationships of minerals.

EPMA data for the Paiting deposit were collected using the Shimadzu-1600 electron microprobe equipped with five wavelength dispersive spectrometers (WDS) at the State Key Laboratory of Ore Deposit Geochemistry, Institute of Geochemistry, Chinese Academy of Sciences. Operating conditions included a 25 kV accelerating voltage, 10 nA beam current with 10-s measurement time, and 10 μm spot size. Standards included marcasite for Fe and S, skutterudite for As, cuprous oxide for Cu, cinnabar for Hg, stibnite for Sb, and native gold and silver for Au and Ag, respectively. Minimum detection limits for all analyzed elements are around 200 ppm.

EPMA data for the Cortez Hills Carlin-type gold deposit, Nevada, were collected by using a JEOL-8900 electron microprobe at UNLV EMiL. Operating conditions included a 20 kV accelerating voltage, 1–2 μm spot size, and 10 nA beam current for major elements with 6-s measurement time and 100 nA beam current for trace elements with 35-s measurement time. Standards include Micro-Analysis Consultants (MAC)-As for As, MAC-FeS_2 for Fe and S, MAC-chalcopyrite for Cu, UNLV standard (CM)-Ag for Ag, CM-HgS for Hg, CM-Sb for Sb, and Geller MicroAnalytical Lab (Gel)-Au for Au, respectively. Minimum detection limits are Fe (~600 ppm), S (~1500 ppm), As (~300 ppm), Cu (~200 ppm), Hg (~100 ppm), Sb (~110 ppm), Au (~100 ppm), and Ag (~100 ppm).

Mineral textures, chemistry, and paragenesis

Paiting gold deposit, Guizhou Province, China

Transects from low-grade to high-grade mudstone in the lower unit of Duliujiang Formation were examined and analyzed using SEM and EPMA to identify the mineral paragenesis. Events recognized at the Paiting deposit include pre-ore formation of host rocks and the subsequent gold hydrothermal event including ore and late-ore stages (Fig. 5).

Pre-ore-stage minerals in low-grade samples (<0.009 g/t gold) include primary host-rock minerals such as abundant calcite (Fig. 6a), detrital quartz, ferroan dolomite, minor disseminated As-free or low-As pyrite, and trace illite (Fig. 5). The sparse, small patches of illite have irregular boundaries and are enclosed by quartz, calcite, or ferroan dolomite. Locally, solid carbon-rich matter fills fractures in low- and high-grade rocks. The As-free or low-As pyrite, commonly 10–50 μm and locally up to 200 μm in diameter, has a typical yellowish-white or yellow color and is commonly subhedral or anhedral and poorly polished (Fig. 6a). Gold, Hg, Cu, Ag, and Sb in these As-free or low-As pyrites were not detected by EPMA, and As was less than 1 wt% (ESM 1). The As-free or low-As pyrite occurs in low- and high-grade samples and commonly is rimmed by ore pyrite in ore.

Calcite, quartz, ferroan dolomite, and trace illite in the low-grade samples are interpreted to have formed during sedimentation and diagenesis and constitute the sedimentary rock. Textures indicate that the carbon-rich matter likely formed prior to gold mineralization. Because the As-free or low-As pyrite lacks enrichments in trace elements typical of ore-stage Carlin-type pyrite, it is likely a pre-ore-stage mineral.

The ore stage is defined as the main stage of gold deposition. Ore-stage minerals include arsenopyrite, arsenian pyrite, pyrrhotite, quartz, dolomite, and illite (Fig. 5). Arsenopyrite and arsenian pyrite, present in medium- and high-grade samples, are the main gold-bearing sulfides, and pyrrhotite is a less common gold-bearing sulfide.

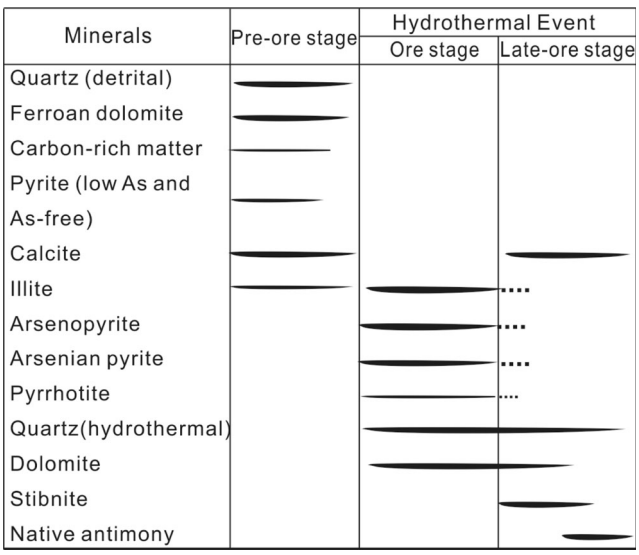

Fig. 5 Mineral paragenesis for the Paiting gold deposit

Arsenopyrite contains variable gold from below the detection limit (DL) of ~200 to 2000 ppm, Sb from below DL to 2300 ppm, Cu from below DL to 1000 ppm, and Hg from below DL to 300 ppm; Ag is below DL (ESM 1). Arsenopyrite, commonly 5 to 40 μm in diameter, has a yellowish to white color, bright reflectivity, and good polish (Fig. 6b). Arsenopyrite is commonly euhedral to subhedral (Fig. 6b, c) and occurs with arsenian pyrite (Fig. 6d). Commonly, arsenopyrite is encompassed by low relief illite (Fig. 6d), quartz, dolomite, and ferroan dolomite (Fig. 6c). Locally, arsenopyrite is encompassed by stibnite (Fig. 6b).

Arsenian pyrite contains gold from below DL (~200 ppm) to 900 ppm, with trace Sb (<~200 to 1800 ppm), Cu (<~200 to 700 ppm), and Hg (<~200 to 800 ppm) (ESM 1). Commonly, arsenian pyrite forms rims, 5 to 30 μm in thickness, that encompass poorly polished As-free or low-As pyrite (Fig. 6d, e) or occurs as euhedral and subhedral crystals (Fig. 6d). The pre-ore cores and ore-stage rims cannot be distinguished by using ore microscopy because the pyrite cores and rims have the same color, relief, and reflectivity (Fig. 6f). However, the core-rim textures are apparent by using backscattered electron (BSE) imaging enhanced with low brightness and high contrast (Fig. 6e). Arsenian pyrite typically has a yellowish-white color, bright reflectivity, and high relief and is well polished (Fig. 6f). Arsenian pyrite is typically encompassed by illite (Fig. 6d), quartz, and dolomite.

Pyrrhotite contains ~1.0 wt% As, and Au ranges from below DL (~200 ppm) to 500 ppm in a few analyses (ESM 1). Pyrrhotite is not common in ore samples. Where present, pyrrhotite occurs as euhedral to subhedral crystals and is associated with carbon-rich matter, and native antimony locally conforms to earlier pyrrhotite (Fig. 6g).

Illite is abundant in high-grade ore, varies from 5 to 20 wt%, and commonly encompasses ore minerals (Fig. 6d). Quartz and dolomite are common gangue minerals that encompass gold-bearing sulfides (Fig. 6c). Zones of jasperoid quartz that replaced calcite display irregular boundaries and commonly contain solid inclusions of calcite. Dolomite, absent from low-grade samples, is intergrown with ferroan dolomite in ore (Fig. 6c).

Arsenopyrite, arsenian pyrite, and pyrrhotite, absent in low-grade samples, occur in medium-grade and high-grade samples and contain gold (ESM 1), indicating that these minerals precipitated during the ore stage. No visible gold has been identified, and the majority of invisible gold is regularly distributed in arsenopyrite and arsenian pyrite based on microprobe analyses, indicating that they are the main gold-bearing minerals. The lack of detection of gold microcrystals by EPMA and the presence of visible rims that have a

consistent brightness under BSE imaging strongly suggest that gold is ionically bound in these minerals. A spatial association and lack of crosscutting textures among gold-bearing arsenopyrite, arsenian pyrite, and pyrrhotite is consistent with formation of these minerals at approximately the same time (Fig. 5). Gold is below DL (<~200 ppm) in some arsenopyrite, arsenian pyrite, and pyrrhotite grains (ESM 1), which may indicate that minor amounts of these minerals continued to precipitate at the beginning of the late-ore stage (Fig. 5). Illite is significantly more abundant in ore than in low-grade samples, and it commonly encompasses ore minerals, consistent with illite precipitation during the ore stage (Fig. 5). Dolomite is absent from low-grade samples but encompasses ore minerals in ore, indicating precipitation during the ore stage. Textures and the presence of tiny calcite inclusions indicate that the irregular jasperoid patches are a product of silicification during the ore stage.

The late-ore stage was recorded by the precipitation of abundant stibnite and minor native antimony (Fig. 5) that encompass or crosscut ore-stage minerals. Stibnite contains from 2.6 to 3.0 wt% As, Au from <~200 to 700 ppm in a few samples, trace Hg (<~200 to 2300 ppm), Fe (<~200 to 1600 ppm), and Cu (<~200 to 500 ppm) (ESM 1). Stibnite commonly occurs in stibnite-native antimony-quartz veins or stibnite-quartz (calcite) veins crosscutting ore (Fig. 6h, i). Stibnite encompasses euhedral quartz (Fig. 6j), rims pyrite (Fig. 6k), rims arsenopyrite (Fig. 6b), encompasses dolomite (Fig. 6l), and occurs as inclusions in dolomite (Fig. 6l).

Native antimony contains Sb from 94.4 to 96.4 wt%, As from 4.5 to 5.0 wt%, Au from below DL (~200 ppm) to 3100 ppm, trace Hg (<~200 to 1000 ppm), and Fe (<~200 to 2800 ppm) (ESM 1). Native antimony is recognizable using both microscopy and SEM. Under the microscope, native antimony has a yellowish-white color and is brighter than stibnite (Fig. 6i, j). In backscattered mode with SEM, it is brighter than any other sulfide mineral present (Fig. 6g, j, k, m, n). Native antimony is commonly anhedral, 1 to 100 μm in diameter, and locally greater than 200 μm. Native antimony rims stibnite (Fig. 6k, n) and pyrite (Fig. 6k) or occurs with pyrrhotite and carbon-rich matter (Fig. 6g). Native antimony commonly forms veinlets or, with stibnite and quartz, forms native antimony-stibnite-quartz veinlets crosscutting ore and quartz-stibnite veins (Fig. 6h, i, m).

Textures strongly support the interpretation that stibnite and native antimony formed during the late-ore stage and native antimony precipitated after stibnite. Some stibnite and native antimony contain trace gold, suggesting that the late-ore fluid contained minor gold. Quartz and calcite, commonly with stibnite, form veinlets crosscutting ore, which indicates that this quartz and calcite precipitated during the late-ore stage. Locally, dolomite containing stibnite inclusions is encompassed by stibnite, which suggests that precipitation of dolomite and stibnite overlapped.

Fig. 6 Minerals and their relationships in the Paiting gold deposit. The *label* in the top right of each image indicates the sample number and gold grade. **a** Low-grade samples contain abundant calcite and disseminated poorly polished pyrite (R&TCPL image). **b** Euhedral arsenopyrite is encompassed by stibnite (RPPL image). **c** Fe-dolomite, dolomite, quartz, and illite occur with arsenopyrite (BSE image with high contrast). Fe-dolomite, dolomite, and quartz have higher relief than illite. Fe-dolomite is brighter than dolomite and quartz. Quartz is darker than dolomite (BSE image). **d** Core-rim textured pyrite and arsenopyrite are disseminated in ore. Illite with low relief is *dark gray*. Quartz has higher relief than illite (BSE image). **e** BSE image with low brightness and high contrast shows core-rim textured pyrite. **f** RPPL image shows the core-rim textured pyrite. **g** Pyrrhotite and native antimony occur with calcite and organic matter (BSE image). **h** Quartz-stibnite-native antimony vein, quartz-stibnite vein and native antimony vein crosscut ore, and quartz-stibnite vein is crosscut by quartz-stibnite-native antimony vein (PSS image). **i** Native antimony vein crosscuts quartz-stibnite-calcite vein (R&TCPL image). **j** Stibnite and native antimony encompass euhedral quartz (R&TCPL image). **k** Stibnite rims pyrite, and native antimony conforms to stibnite and pyrite (BSE image). **l** Stibnite encompasses dolomite, which contains solid inclusions of stibnite (BSE image). **m** Native antimony vein crosscuts ore (BSE image). **n** Native antimony conforms to stibnite (BSE image). *R&TCPL* reflected and transmitted crossed polarized light, *RPPL* reflected plane polarized light, *BSE* backscattered electron, *PSS* polished section scan, *asp* arsenopyrite, *As-py* arsenian pyrite, *cc* calcite, *crm* carbon-rich matter, *dol* dolomite, *Fe-dol* Fe-dolomite, *ill* illite, *po* pyrrhotite, *py* pyrite, *qtz* quartz, Sb^0 native antimony, *stb* stibnite

The physicochemical parameters of ore formation in the Paiting deposit are summarized in Table 1. The sulfur and oxygen fugacities during the ore and late-ore stages at the Paiting deposit can be estimated using sulfur fugacity-oxygen fugacity-temperature phase diagrams calculated for ore-stage minerals in the Twin Creeks Carlin-type gold deposit in Nevada (Simon et al. 1999). The mineralization temperature in the Paiting deposit ranged from 290 to 200 °C during the ore stage and from 220 to 110 °C during the late-ore stage, based on bitumen reflectance analyses and homogenization temperatures of fluid inclusions in quartz from gold-rich zones (Chen et al., Guizhou University of Industry, unpublished report 1998). Using the ore-stage pyrite-arsenopyrite-pyrrhotite assemblage (Fig. 5) and temperatures from 290 to 200 °C, the ore-stage log $fS_{2(g)}$ can be inferred as about −10.5 to −16 (Fig. 7). The late-ore-stage log $fS_{2(g)}$ can be inferred as −14 to −25.5 based on the late-ore-stage mineral assemblage of stibnite-native antimony (Fig. 5) and temperatures from 220 to 110 °C.

Based on the indicated sulfur fugacities and stable mineral assemblages, the log $fO_{2(g)}$ of the ore and late-ore stages can be inferred. The ore-stage log $fO_{2(g)}$ ranges from −36 to at least −45 (Fig. 8a) for the pyrite-arsenopyrite-pyrrhotite assemblage (Fig. 5). The late-ore-stage native antimony-stibnite assemblage is inferred to have formed under log $fO_{2(g)}$ conditions of −48.5 to at least −55 (Fig. 8b).

The solubilities of antimony and aqueous antimony species are mainly controlled by temperature, pH, $fO_{2(g)}$, and $fS_{2(g)}$ (Williams-Jones and Normand 1997). Antimony is transported

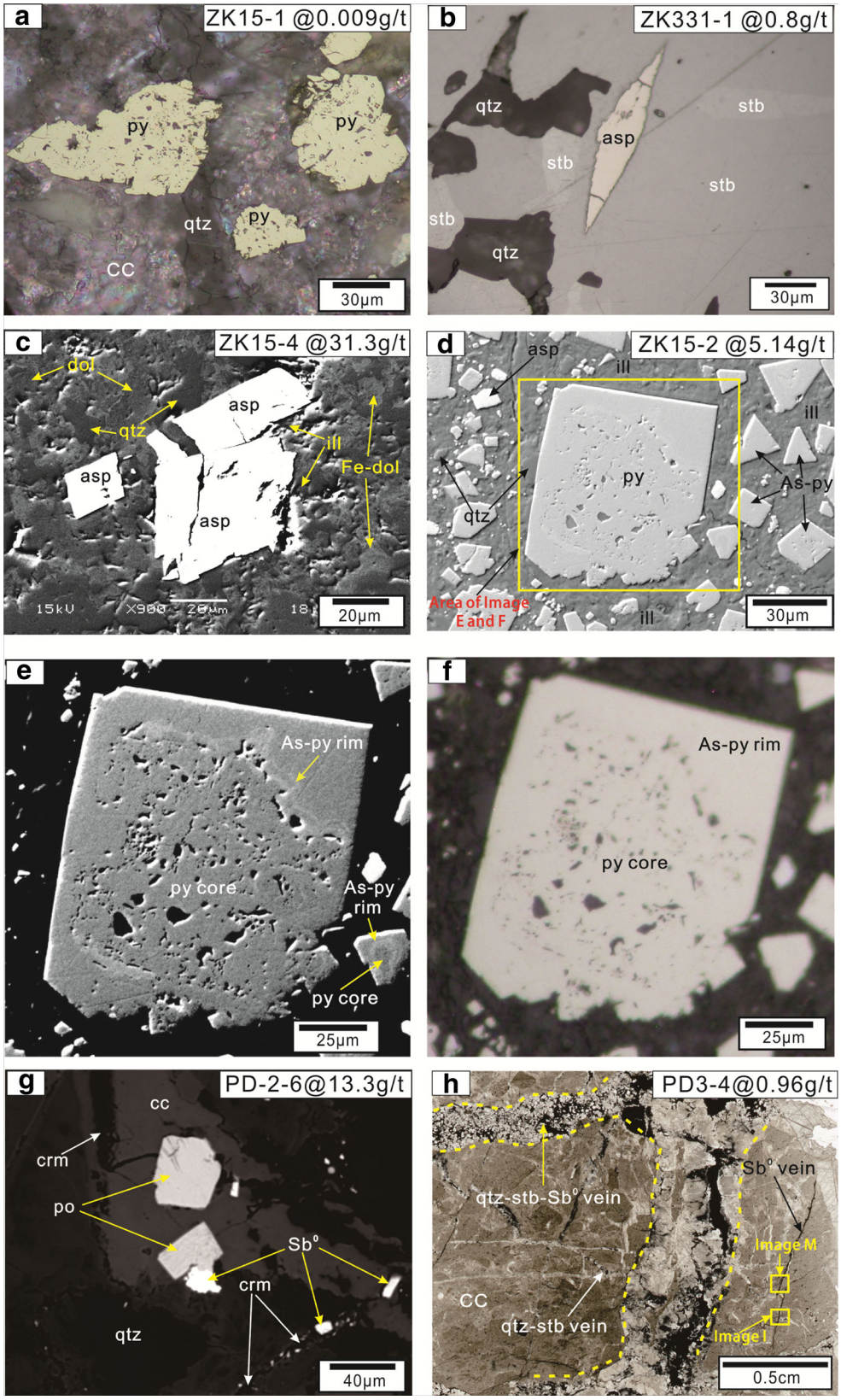

principally as $Sb(OH)_3^0$ (Wood et al. 1987; Shikina and Zotov 1991), as $Sb_2S_2(OH)_2^0$ at low pH and intermediate fO_2 (Krupp 1988; Spycher and Reed 1989), as $HSb_2S_4^-$ at intermediate pH of 6–7.7 and intermediate fO_2 (Krupp 1988; Williams-Jones

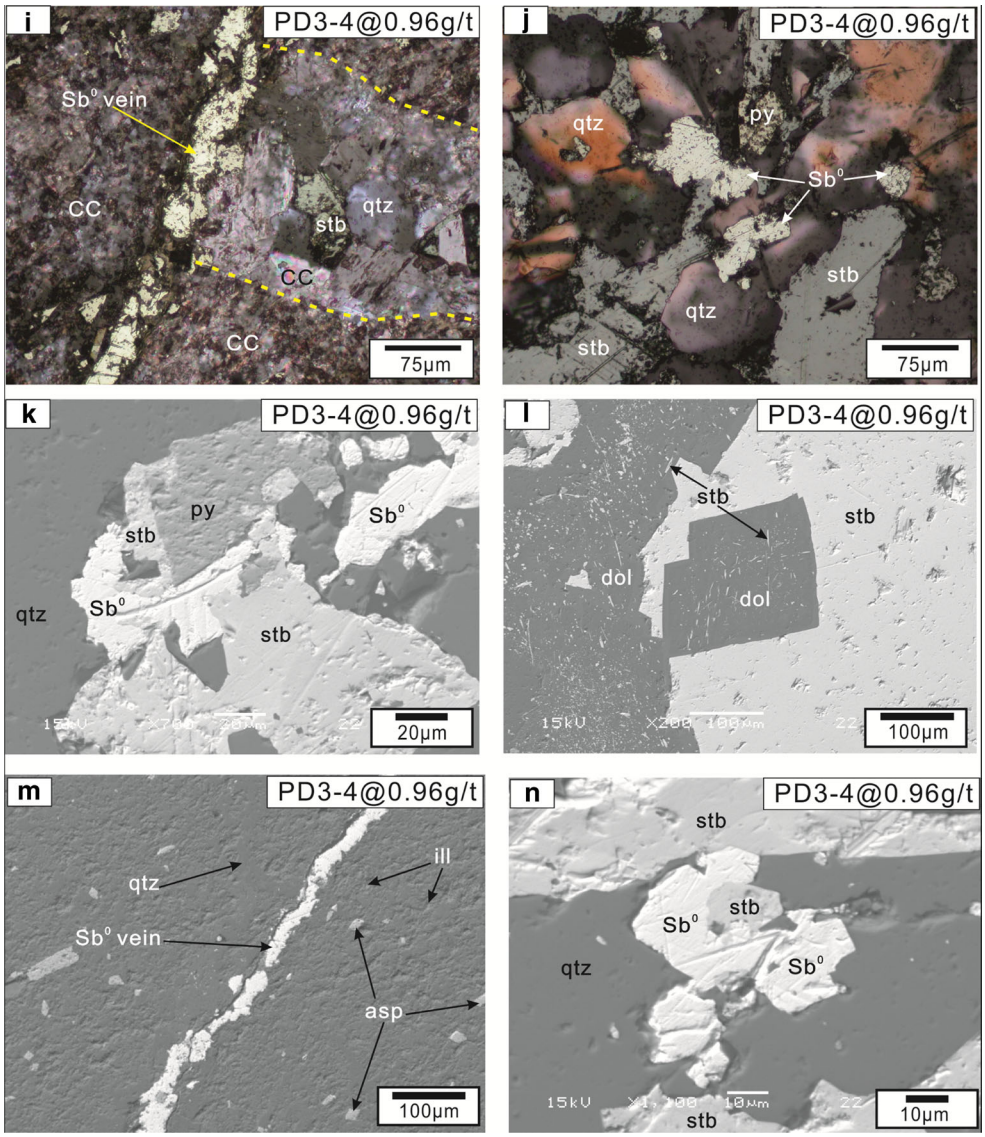

Fig. 6 (continued)

and Normand 1997), or as $Sb(OH)_4^-$ at high pH conditions of >10 (Williams-Jones and Normand 1997) (Fig. 9). Williams-Jones and Normand (1997) determined mineral stability relationships and antimony solubility in the system Fe-Sb-S-O. Applied to the Paiting deposit that exhibits carbonate-stable alteration, the ore fluid pH was likely near neutral at ~5.5 at 200 °C (Barnes 1979) to alkaline. The solubility of antimony at neutral to alkaline pH approaches hundreds of ppm at log $fO_{2(g)} > -36$ (Fig. 9), where antimony is likely transported as $Sb(OH)_3^0$. As log $fO_{2(g)}$ decreased from −36 to −50, the

Table 1 Physicochemical parameters of Paiting gold deposit

Physicochemical parameter	Ore stage	Late-ore stage	Source of data
Temperature/°C	290 to 200	220 to 110	Bitumen reflectance analyses and fluid inclusion studies, Chen et al., Guizhou University of Industry, unpublished report 1998
Log $fS_{2(g)}$	−10.5 to −16	−14 to −25.5	Ore- and late-ore-stage mineral assemblages from this study; $fS_{2(g)}$-temperature phase equilibria
Log $fO_{2(g)}$	−36 to −45	−48.5 to −55	Ore- and late-ore-stage mineral assemblages from this study; $fO_{2(g)}$-$fS_{2(g)}$ phase equilibria

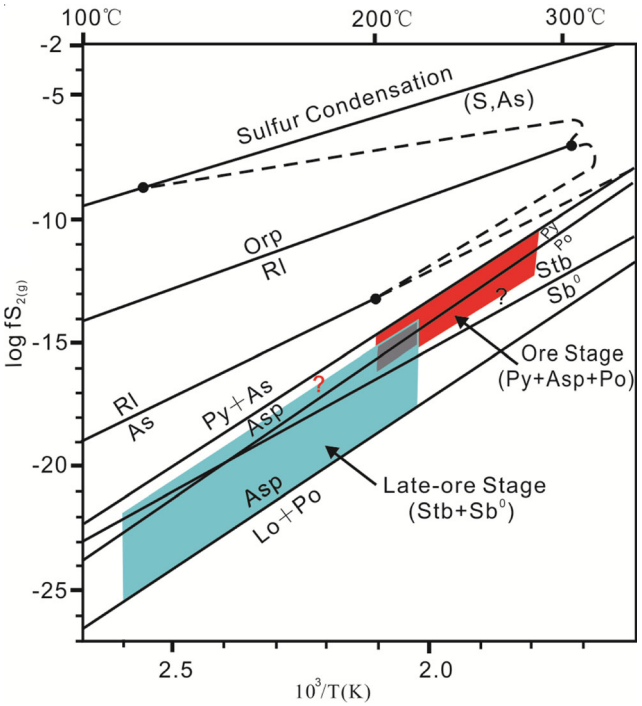

Fig. 7 Temperature versus log $fS_{2(g)}$ diagram showing stability fields of minerals present in ore and late-ore stages at the Paiting deposit (modified from Simon et al. 1999). *Red* represents the stability field of ore-stage minerals pyrite, arsenopyrite, and pyrrhotite, and *light blue* represents the stability field of late-ore-stage minerals stibnite and native antimony. *Boundary with question mark* means that the exact location of the sulfur fugacity boundary is unknown but is somewhere between the two nearest boundaries. *As* arsenic, *Asp* arsenopyrite, *Lo* loellingite, *Orp* orpiment, *Po* pyrrhotite, *Py* pyrite, *Rl* realgar, *S* sulfur, Sb^0 native antimony, *Stb* stibnite

solubility of antimony decreased to 0.001 ppm, and antimony transport likely switched to $HSb_2S_4^-$ at this reduced oxygen fugacity and neutral to alkaline pH (Fig. 9).

Cortez Hills Carlin-type gold deposit, Nevada, USA

Ore pyrite (Fig. 10a, b) in the Cortez Hills deposit contains 1000 to 3200 ppm Au and is enriched in As (4.2 to 12.9 wt%), Cu (2000 to 12200 ppm), Hg (1800 to 11600 ppm), and Sb (200 to 1000 ppm) (ESM 1). Silver was below DL in all analyses. The concentrations of As, Cu, and Hg in Cortez Hills pyrite are approximately 2.3, 15.7, and 16.7 times higher than they are in Paiting ore pyrite (ESM 1). Ore pyrite has a golden yellow color (Fig. 10a) and is soft and has a poor polish (Fig. 10b). The ore pyrite, with irregular, feathery outer edges, has earned the name "fuzzy" pyrite (Cline et al. 2005). Ore pyrite commonly rims euhedral, well-polished pre-ore pyrite, or forms small, commonly 1 to 10 μm in diameter, individual spheroidal pyrite disseminated in ore (Fig. 10a, b). The ore pyrite rims, commonly1 to 10 μm in thickness, can be observed easily on the microscope (Fig. 10a) and with BSE imaging (Fig. 10b). The gangue minerals that consistently encompass the ore pyrite are illite and jasperoid (Fig. 10a, b). In high-grade ore slabs, blue epoxy fills abundant space that was formerly pore space in the rock (Fig. 10a).

The ore pyrite and alteration in the Cortez Hills deposit exhibit characteristics that are typical of Carlin-type gold deposits in Nevada (Cline et al. 2005). The fuzzy arsenian pyrite is enriched in As, Cu, and Hg in addition to Au and is the typical gold-bearing sulfide. Decarbonatization removed former carbonate minerals and, where not replaced by other minerals, left much pore space. Silicification in the form of jasperoid replaced carbonate minerals, and argillization is represented by abundant illite encompassing ore pyrite and jasperoid.

Discussion

Precipitation of native antimony in the Paiting deposit

Krupp and Seward (1990) and Normand et al. (1996) concluded that CH_4 is the predominant carbonic vapor phase in equilibrium with native antimony, with native antimony precipitating from reduced fluids dominated by CH_4. Williams-Jones and Normand (1997) described stibnite deposits throughout the world and determined that most stibnite deposits that contain native antimony occur in black shale. The Paiting host rocks are enriched in carbon-rich matter (Fig. 6g); the Cambrian Bianmachong Formation (∈1b) is dominated by black carbonaceous shale (Fig. 4), and the Wuxun Formation (∈1w) contains carbonaceous mudstone (Fig. 4), consistent with fluid inclusions that contain up to 4.0 mol% CH_4 (Li et al. 2002). Black carbonaceous shale and/or carbon-rich matter likely provided carbon for CH_4 in the hydrothermal fluid and also produced reducing conditions consistent with precipitation of native antimony.

Temperature and sulfur fugacity are two important factors controlling the solubility of antimony and the stability of stibnite (Williams-Jones and Normand 1997; An and Zhu 2010). During the ore stage at the Paiting deposit, conditions (Table 1) are consistent with antimony transport as $Sb(OH)_3^0$ and gold transport as $AuHS^0$ (Stefansson and Seward 2004). As arsenopyrite, arsenian pyrite, and pyrrhotite precipitated during the ore stage at temperatures between 290 and 200 °C, the vast majority of gold in the deposit was likely captured as Au^+ ions within arsenopyrite and arsenian pyrite. The precipitation of arsenopyrite and other sulfide minerals reduced the concentration of available reduced sulfur in the ore fluid. Over time, the ore stage transitioned to a late-ore stage with a log sulfur fugacity between −14 and −25.5, a log oxygen fugacity between −48.5 and −55, and an ore fluid temperature between 220 and 110 °C. This transition caused the solubility of antimony to decrease significantly from

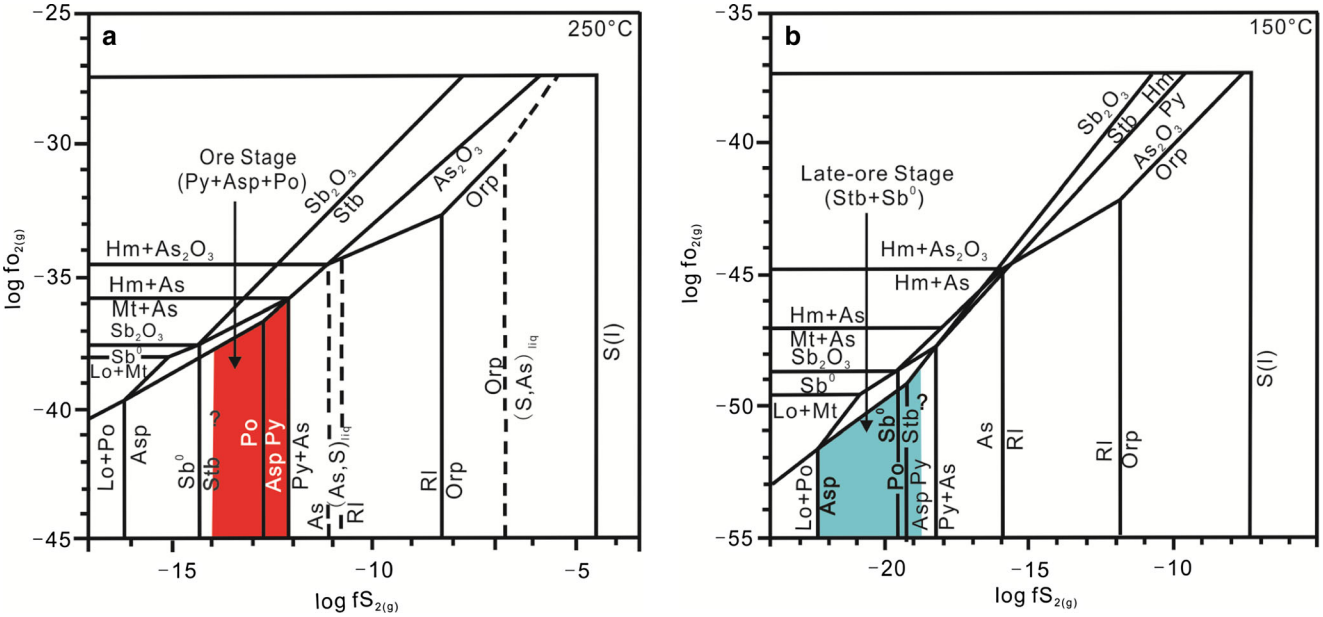

Fig. 8 **a** Log $fS_{2(g)}$ versus log $fO_{2(g)}$ diagram showing the stability fields of mineral assemblages in the ore stage at 250 °C (modified from Simon et al. 1999). *Red* represents the stability field of ore-stage minerals pyrite, arsenopyrite, and pyrrhotite. The exact location of the sulfur fugacity boundary shown with a *question mark* is not known, but the boundary is located between the two nearest boundaries. **b** Log $fS_{2(g)}$ versus log $fO_{2(g)}$ diagram showing stability fields of minerals in the late-ore stage at 150 °C (modified from Simon et al. 1999). *Light blue* represents the stability field of late-ore-stage minerals stibnite and native antimony. The exact location of the sulfur fugacity boundary shown with a *question mark* is unknown, but the boundary is located between the two nearest boundaries. *As* arsenic, *Asp* arsenopyrite, *Hm* hematite, *Lo* loellingite, *Mt* magnetite, *Orp* orpiment, *Po* pyrrhotite, *Py* pyrite, *Rl* realgar, *S* sulfur, *Sb^0* native antimony, *Stb* stibnite

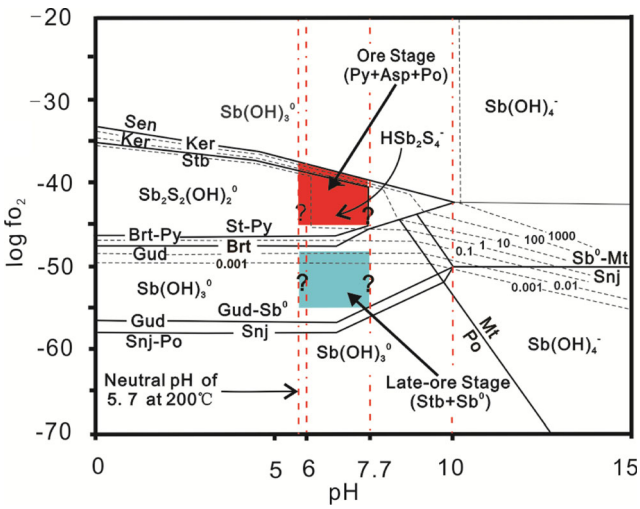

Fig. 9 Log $fO_{2(g)}$ versus pH diagram at 200 °C and $\Sigma\alpha s = 0.01$, showing contours of antimony solubility in ppm (*black dashed lines*). Also shown are the distribution of the dominant Sb species (note that the species $HSb_2S_4^-$ is limited to pH conditions between 6.0 to 7.7 and $Sb(OH)_4^-$ to pH >10) and stability fields of minerals (*black solid lines*) in the system Fe-Sb-S-O (modified from Williams-Jones and Normand 1997). The fields of ore-stage and late-ore-stage minerals in the Paiting gold deposit are shown. *Red* represents the stability field of ore-stage minerals pyrite, arsenopyrite, and pyrrhotite, and *light blue* represents the stability field of late-ore-stage minerals stibnite and native antimony. Poorly defined boundaries are indicated with a *question mark*. *Brt* berthierite, *Gud* gudmundite, *Hm* hematite, *Ker* kermesite, *Mt* magnetite, *Orp* orpiment, *Po* pyrrhotite, *Py* pyrite, *Sb^0* native antimony, *Sen* senarmontite, *Snj* seinajokite, *Stb* stibnite

hundreds of ppm to <0.001 ppm, causing precipitation of stibnite and native antimony.

Precipitation of native antimony in the late-ore stage indicates that the late-ore fluid in the Paiting deposit differs from what has been reported in other sediment-hosted gold deposits in southwestern Guizhou and Nevada. Liu et al. (2007) suggested that in southwestern Guizhou, China, the sulfur and oxygen fugacities increased from the ore stage to late-ore stage based on the mineral paragenesis of sediment-hosted gold deposits. Simon et al. (1999) concluded that in the Twin Creeks Carlin-type gold deposit, Nevada, the log sulfur fugacity in the ore fluid decreased from about −6 to −16 from the ore stage to the late-ore stage. However, in the Paiting gold deposit, the drops in log sulfur and oxygen fugacities were dramatic, possibly from about −10.5 to −25.5 and −36 to −55, respectively. These values are unusually low, and under these conditions, only stibnite and native antimony, rather than realgar and orpiment, were stable (Figs. 7 and 8). Thus, although the content of arsenic reached 5.0 wt% in native antimony at Paiting (ESM 1), minerals such as realgar and orpiment, which are common in the Nevada Carlin-type gold deposits and in the southwestern Guizhou province sediment-hosted gold deposits, did not precipitate.

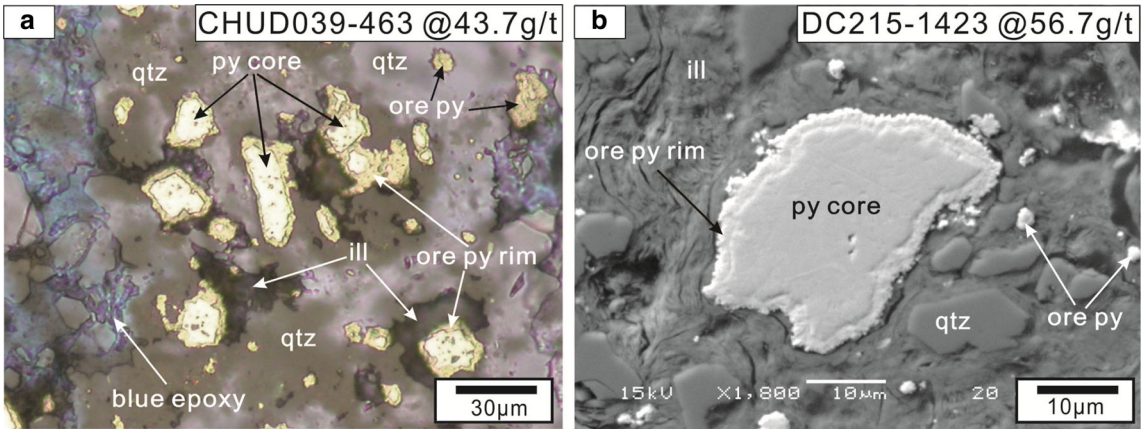

Fig. 10 Typical ore and alteration minerals in the Cortez Hills Carlin-type gold deposit, Nevada. The *label* in the top right of each image indicates the drill hole number, sampling depth (feet), and gold grade. **a** Ore-stage fuzzy pyrites rim pre-ore pyrite grains, ore pyrites are encompassed by illite and quartz, and blue epoxy fills former open space (R&TPPL image). **b** Pre-ore pyrite core is rimmed by ore-stage fuzzy pyrite, and ore pyrites are encompassed by illite and quartz (BSE image). *R&TPPL* reflected and transmitted plane polarized light, *BSE* backscattered electron, *py* pyrite, *ill* illite, *qtz* quartz

Comparison of the Paiting gold deposit with Nevada Carlin-type gold deposits

Our examination of ore and late-ore-stage minerals and alteration in the Paiting and Cortez Hills deposits determined that the Paiting gold deposit exhibits some characteristics of Nevada Carlin-type gold deposits, as well as significant differences. Similarities include the following: (1) Orebodies exhibit both structural and stratigraphic controls, are preferentially hosted by limestone and mudstone, and are related to faults that were ore fluid conduits. (2) Invisible gold is ionically bound in arsenian pyrite.

However, there are also important differences in ore, late-ore and alteration minerals, and ore fluid in the two districts. The gold-bearing sulfide mineral in the Nevada deposits is dominantly arsenian pyrite, whereas in the Paiting deposit, gold is in arsenopyrite, arsenian pyrite, and trace pyrrhotite, and some of the late-ore-stage stibnite and native antimony also contain trace gold. In addition, the morphology and chemistry of gold-bearing arsenian pyrite are significantly different. The Paiting ore-stage arsenian pyrite is commonly euhedral to subhedral, and typical Nevada fuzzy gold-bearing pyrites are not observed. Although gold-bearing sulfides in both the Paiting and Nevada deposits are enriched in trace As, Cu, and Hg, the concentrations of these elements in Paiting gold-bearing sulfide minerals are much lower than in Nevada pyrites.

Alteration in the Paiting gold deposit differs significantly from the Nevada deposits. Decarbonatization, a major alteration process in Nevada, is not important in the Paiting deposit as shown by the common occurrence of gold-bearing arsenopyrite and pyrite with stable dolomite and ferroan dolomite in addition to jasperoid and variable illite. Precipitation of dolomite is an important ore-stage alteration process in the Paiting deposit, whereas ore-stage dolomitization in Nevada deposits is not reported and removal of carbonate dominates alteration processes. The presence of stable carbonate minerals in Paiting ore indicates that ore fluids in the Paiting deposit were less acidic than Nevada ore fluids.

Late-ore-stage minerals in the Paiting deposit exhibit differences from the Nevada deposits. Orpiment and realgar, the typical late-ore-stage mineral in Nevada deposits, did not occur in the Paiting deposit; instead, abundant stibnite with minor native antimony typifies the Paiting late-ore-stage minerals.

Igneous rocks are not observed in the Paiting deposit area, but deposits in Nevada are spatially and temporally associated with magmatism (Cline et al. 2005; Muntean et al. 2011). The Nevada Carlin-type gold deposits formed from ~42 to 36 Ma (Hofstra et al. 1999) and young to south (Muntean et al. 2011), which temporally and spatially coincides with the southward sweep of magmatism that was initiated by Farallon plate roll-back and delamination (Humphreys 1995; Ressel and Henry 2006; Muntean et al. 2011).

Fluid inclusion studies indicate that Paiting ore fluids differed from Nevada ore fluids in that the former was enriched in CH_4 (4.0 mol%) and CO_2 (1.6 mol%), and temperatures were hotter (200–290 °C) (Chen et al., Guizhou University of Industry, unpublished report 1998; Li et al. 2002). Nevada ore fluids are of moderate temperature (180–240 °C), low salinity (<5 wt% NaCl equiv), somewhat low pH (≤5), and contained <4 mol% CO_2, <0.4 mol% CH_4, and >0.01 mol% H_2S (Hofstra and Cline 2000; Cline et al. 2005; Lubben et al. 2012).

Although host rocks and ionic gold in arsenian pyrite at the Paiting and Nevada deposits are quite similar, the ore- and late-ore-stage minerals, alteration, and ore fluid chemistry and temperature display significant differences, which

indicate that the processes that produced the minerals and deposits were different. In the Nevada deposits, fluid-rock reaction between an acidic fluid and reactive rock caused decalcification and precipitation of gold-bearing arsenian pyrite, jasperoid, and illite. During the late-ore stage, realgar, orpiment, calcite, rare stibnite, and quartz precipitated in response to cooling and collapse of the hydrothermal system (Hofstra and Cline 2000; Cline et al. 2005). In the Paiting deposit, a neutral or perhaps alkaline and CH_4- and CO_2-rich ore fluid at higher temperature precipitated gold-bearing arsenopyrite, arsenian pyrite, pyrrhotite, dolomite, jasperoid, and illite. During the late-ore stage, sulfur and oxygen fugacities decreased significantly, and stibnite and native antimony containing trace gold precipitated.

Studies of other sediment-hosted gold deposits in southwestern Guizhou Province also indicate that gold mineralization was accompanied by precipitation of dolomite, and these deposits formed from ore fluids enriched in CO_2 at a higher temperature and pressure than the Nevada deposits. Abundant ore-stage dolomite encompassing ore pyrite was identified at both the Jinfeng and Shuiyindong deposits (Zhuojun Xie unpublished data). Fluid inclusion studies at Jinfeng indicate that ore fluids were CO_2-rich (7–75 mol%), of moderately high temperature (240–300 °C), and trapped under pressures of 1.5 to 2.3 kbar (Zhang et al. 2003). Fluid inclusion research at Shuiyindong suggests that this deposit formed from moderate temperature (190–230 °C), CO_2-bearing (6.3–8.4 mol%) aqueous fluids trapped at pressures of 0.45–1.15 kbar (Su et al. 2009). Cline et al. (2013) applied a pressure correction to the pre main ore-stage inclusions, yielding trapping temperatures of about 220–345 °C.

The dolomite-stable alteration and higher temperature and pressure ore fluids enriched in CO_2, identified in the Paiting and other Guizhou sediment-hosted gold deposits, are different from conditions typical of formation of Carlin-type deposits in Nevada. They are, however, similar to formation conditions of orogenic gold deposits. Groves et al. (1998) and Goldfarb et al. (2005) summarized the characteristics of orogenic deposits and stressed that these deposits commonly formed at temperatures between 250 and 400 °C and depths between 2 and 20 km, conditions that are higher in temperature and greater in depth than conditions typical of Carlin-type deposits (Cline et al. 2005). They also emphasized that orogenic deposits commonly formed from near-neutral and slightly reduced ore fluids that were enriched in CO_2 (between 4 and 30 mol%) and that ore-stage carbonate is typical of hydrothermal alteration in orogenic deposits.

Collectively, our results indicate that the Paiting and other sediment-hosted gold deposits in Guizhou Province formed at pressure-temperature-chemistry conditions intermediate to the shallower and lower pressure-temperature Carlin-type and the more deeply formed and higher pressure-temperature orogenic systems, which explains why the Guizhou deposits have similarities to both Carlin-type and orogenic gold deposits. The neutral or perhaps alkaline ore fluids with high concentration of CO_2 in the Guizhou ore fluid allowed stabilization of dolomite during the ore stage. The higher temperatures and pressures of the Guizhou ore fluids, as compared to Nevada ore fluids, are consistent with precipitation of ore-stage arsenopyrite and pyrrhotite in the Guizhou deposits.

Conclusions

The Paiting gold deposit has similar and different characteristics compared to the Carlin-type deposits of Nevada. Both are hosted by sedimentary rocks and both contain ionically bound gold in arsenian pyrite. Main differences include lower concentrations of As, Cu, and Hg in subhedral to euhedral gold-bearing sulfide minerals and the presence of dolomite-stable alteration in the Pating deposit. Abundant late-ore-stage stibnite and minor native antimony occur at Pating, but realgar and orpiment are lacking. Also, Paiting ore fluids had higher temperatures and transported higher concentrations of CH_4 and possibly CO_2 than typical Carlin ore fluids in Nevada. The carbonate-stable alteration that resulted from CO_2-bearing ore fluids with temperatures in excess of 250 °C is characteristic of orogenic deposits rather than Carlin-type deposits. Thus, the Paiting deposit exhibits some similarities to both typical Carlin-type deposits and orogenic gold deposits, suggesting that this deposit formed at pressure-temperature-chemistry conditions intermediate between these two major ore styles.

Acknowledgments We are grateful to the No. 1 Corps of Non-ferrous Geological Exploration of Guizhou Province and Barrick Gold Corporation for access to samples from the Paiting deposit, Guizhou Province, China, and the Cortez Hills deposit, Nevada, USA. Shijun Xia is thanked for geologic guidance during the fieldwork at the Paiting deposit. Minghua Ren, Michael Strange, Wenqing Jiang, and Shaohua Dong are thanked for assistance with SEM and electron microprobe analyses. We are also indebted to Bernd Lehmann, Karen Kelley, Sheng-Rong Li, John Muntean, and Thomas Wagner for comments and suggestions that have improved this paper. This work was supported by the 973 Program (2014CB440905), National Science Foundation of China (41230316), CAS/SAFEA International Partnership Program for Creative Research Teams (Intraplate Mineralization Research Team: KZZD-EW-TZ-20), 12th five-year project of State Key Laboratory of Ore Deposit Geochemistry (SKLODG-ZY125-01), China Scholarship Council, and Scholarship from Institute of Geochemistry, Chinese Academy of Sciences.

References

An F, Zhu YF (2010) Native antimony in the Baogutu gold deposit (west Junggar, NW China): its occurrence and origin. Ore Geol Rev 37: 214–223

Arbonies DG, Creel KD, Jackson ML (2011) Cortez hills lower zone discovery and geologic update. In: Steininger R, Pennell B (eds)

Great basin evolution and metallogeny. Geological Society of Nevada Symposium Volume, Reno, pp 447–462

Arehart GB (1996) Characteristics and origin of sediment-hosted gold deposits: a review. Ore Geol Rev 11:383–403

Barnes HL (1979) Solubilities of ore minerals. In: Barnes HL (ed) Geochemistry of hydrothermal ore deposits, 2nd edn. University Park, Pennsylvania, pp 404–460

Barrick Gold Corporation (2014) Barrick reports fourth quarter and full year 2014 results.http://www.barrick.com/investors/news/news-details/2015/Barrick-Reports-Fourth-Quarter-and-Full-Year-2014-Results/default.aspx

Bellot JP (2003) The Biards Sb-Au bearing zone (Massif Central, France): an indicator of crustal-scale transcurrent tectonics guiding late Variscan collapse. Econ Geol 98:1427–1447

Cail T, Cline JS (2001) Alteration associated with gold mineralization at the Getchell Carlin-type gold deposit, northern Nevada, USA. Econ Geol 96:1343–1359

Chen MH, Mao JW, Bierlein FP, Norman T, Uttley PJ (2011) Structural features and metallogenesis of the Carlin-type Jinfeng (Lannigou) gold deposit, Guizhou Province, China. Ore Geol Rev 43:217–234

Clark L (2012) Ore and gangue mineral paragenesis of the Cortez Hills Carlin-type gold deposit, Nevada: evidence for coincident high-grade gold deposition and collapse brecciation. Dissertation, University of Nevada Las Vegas

Cline JS, Hofstra AH (2000) Ore-fluid evolution at the Getchell Carlin-type gold deposit, Nevada, USA. Eur J Mineral 12:195–212

Cline JS, Hofstra AH, Muntean JL, Tosdal RM, Hickey KA (2005) Carlin-type gold deposits in Nevada: critical geologic characteristics and viable models. In: Hedenquist JW, Thompson JFH, Goldfarb RJ, Richards JP (eds) Economic geology 100th anniversary volume. Society of Economic Geologists, Inc, Littleton, pp 451–484

Cline JS, Muntean JL, Gu XX, Xia Y (2013) A comparison of Carlin-type gold deposits: Guizhou province, golden triangle, southwest China, and northern Nevada, USA. Earth Sci Front 20:1–18

Dong GG (2007) Geological characteristics of the Paiting gold deposit in Southeast Guizhou. Acta Miner Sin (supl.): 96–97 (in Chinese)

Fan EC (2010) Ore-controlling factors and prospecting direction of Paiting gold deposit in Danzhai, Guizhou. Acta Geol Sin 24:322–327 **(in Chinese with English abstract)**

Gao ZM, Li HY, Yang ZS, Tao Y, Luo TY, Liu XF, Xia Y, Rao WB (2002) Metallogenic and ore prospecting of the main gold deposits, Guizhou Province and Yunnan Province. Geological Publishing House, Beijing **(in Chinese with English abstract)**

Goldfarb RJ, Baker T, Dube B, Groves DI, Hart CJR, Gosselin P (2005) Distribution, character and genesis of gold deposits in metamorphic terranes. In: Hedenquist JW, Thompson JFH, Goldfarb RJ, Richards JP (eds) Economic geology 100th anniversary volume. Society of Economic Geologists, Inc, Littleton, pp 407–450

Groves DI, Goldfarb RJ, Gebre-Mariam M, Hagemann SG, Robert F (1998) Orogenic gold deposits: a proposed classification in the context of their crustal distribution and relationship to other gold deposit types. Ore Geol Rev 13:7–27

Hofstra AH, Cline JS (2000) Characteristics and models for Carlin-type gold deposits. In: Hagemann SG, Brown PE (eds) Gold in 2000. Reviews in economic geology. Society of Economic Geologists Inc, Littleton, pp 163–220

Hofstra AH, Leventhal JS, Northrop HR, Landis GP, Rye RO, Birak DJ, Dahl AR (1991) Genesis of sediment-hosted disseminated gold deposits by fluid mixing and sulfidization: chemical-reaction-path modeling of ore-depositional processes documented in the Jerritt Canyon district, Nevada. Geology 19:36–40

Hofstra AH, Snee LW, Rye RO, Folger HW, Phinisey JD, Loranger RJ, Dahl AR, Naeser CW, Stein HJ, Lewchuk M (1999) Age constraints on Jerritt Canyon and other Carlin-type gold deposits in the western United States: relationship to mid-tertiary extension and magmatism. Econ Geol 94:769–802

Hu RZ, Su WC, Bi XW, Tu GZ, Hofstra AH (2002) Geology and geochemistry of Carlin-type gold deposits in China. Miner Deposita 37: 378–392

Humphreys ED (1995) Post Laramide removal of the Farallon slab, western United States. Geology 23:987–990

Jackson M, Arbonies D, Creel K (2011) Architecture of the Cortez hills breccia body. In: Steininger R, Pennell B (eds) Great basin evolution and metallogeny. Geological Society of Nevada Symposium Volume, Reno, pp 14–22

Krupp RE (1988) Solubility of stibnite in hydrogen sulfide solutions speciation and equilibrium constants from 25 to 350°C. Geochim Cosmochim Acta 52:3005–3015

Krupp RE, Seward TM (1990) Transport and deposition of metals in the Rotokawa geothermal system, New Zealand. Miner Deposita 25: 73–81

Li HY, Gao ZM, Yang ZS, Luo TY, Rao WB (2002) Geochemical characteristics of the Carlin-type gold deposits in Danzhai, Guizhou (in Chinese). Chin J Geol 37:1–7 **(in Chinese with English abstract)**

Li CY, Liu YP, Zhang Q, Pi DH, Zhang WL, Chen J (2005) Discovery of antimony and distribution on characteristics of associated elements in Huize Pb-Zn deposit. Mineral Deposita 24:52–60 **(in Chinese with English abstract)**

Liu JJ, Yang D, Liu JM, Liu ZJ, Yang Y, Mao GJ, Zhen MH (2007) Mineralogical characteristics of native arsenic and tracing the metallogenic physicochemical condition in Carlin-type gold deposits. Earth Sci Front 14:158–166 **(in Chinese with English abstract)**

Lubben JD, Cline JS, Barker SLL (2012) Ore fluid properties and sources from quartz-associated gold at the Betze-Post Carlin-type gold deposit, Nevada, United States. Econ Geol 107:1351–1385

Muntean JL, Cline JS, Simon AC, Longo AA (2011) Magmatic-hydrothermal origin of Nevada's Carlin-type gold deposits. Nat Geosci 4:122–127

Normand C, Gauthier M, Jebrak M (1996) The Quebec antimony deposit: an example of gudmundite-native antimony mineralization in the ophiolitic mélange of the southeastern Quebec Appalachians. Econ Geol 91:149–163

Palenik CS, Utsunomiya S, Reich M, Kesler SE, Wang L, Ewing RC (2004) "Invisible" gold revealed: direct imaging of gold nanoparticles in a Carlin-type deposit. Am Mineral 89:1359–1366

Reich M, Kesler SE, Utsunomiya S, Palenik CS, Chryssoulis SL, Ewing RC (2005) Solubility of gold in arsenian pyrite. Geochim Cosmochim Acta 69:2781–2796

Ressel MW, Henry CD (2006) Igneous geology of the Carlin trend, Nevada: development of the Eocene plutonic complex and significance for Carlin-type gold deposits. Econ Geol 101:347–383

Rytuba JJ (1985) Geochemistry of hydrothermal transport and deposition of gold and sulfide minerals in Carlin-type gold deposit. US Geol Surv Bull 1646:27–34

Shikina ND, Zotov AV (1991) Thermodynamic parameters of $Sb(OH)_3^0$ (sol) up to 723.15K and 1000 bar. Geochem Int 28:97–103

Simon G, Kesler SE, Chryssoulis S (1999) Geochemistry and textures of gold-bearing arsenian pyrite, Twin Creeks, Nevada: implications for deposition of gold in Carlin-type deposits. Econ Geol 94:405–422

Spycher NF, Reed MH (1989) As (III) and Sb (III) sulfide complexes: an evaluation of stoichiometry and stability from existing experimental data. Geochim Cosmochim Acta 53:2185–2194

Stefansson A, Seward TM (2004) Gold (I) complexing in aqueous sulphide solution to 500°C at 500 bar. Geochim Cosmochim Acta 68: 4121–4143

Su WC, Xia B, Zhang HT, Zhang XC, Hu RZ (2008) Visible gold in arsenian pyrite at the Shuiyindong Carlin-type gold deposit, Guizhou, China: implications for the environment and processes of ore formation. Ore Geol Rev 33:667–679

Su WC, Heinrich CA, Pettke T, Zhang XC, Hu RZ, Xia B (2009) Sediment-hosted gold deposits in Guizhou, China: products of wall-rock sulfidation by deep crustal fluids. Econ Geol 104:73–93

Su WC, Zhang HT, Hu RZ, Xi G, Xia B, Chen YY, Zhu C (2012) Mineralogy and geochemistry of gold-bearing arsenian pyrite from the Shuiyindong Carlin-type gold deposit, Guizhou, China: implications for gold depositional processes. Mineral Deposita 47:653–662

Tan YJ (2001) Native arsenic in the Carlin-type gold deposits. Mineral Resour Geol 87:699–704 **(in Chinese with English abstract)**

Thorne KG, Lentz DR, Hoy D, Fyffe LR, Cabri LJ (2008) Characteristics of mineralization at the main zone of the Clarence stream gold deposit, southwestern New Brunswick, Canada: evidence for an intrusion-related gold system in the Northern Appalachian orogen. Explor Min Geol 17:13–49

Wang ZP (2013) Genesis and dynamic mechanism of the epithermal ore deposits, SW Guizhou, China-A case study of gold and antimony deposits. Dissertation, University of Chinese Academy of Sciences (in Chinese with English abstract)

Williams-Jones AE, Normand C (1997) Controls of mineral parageneses in the system Fe-Sb-S-O. Econ Geol 92:308–324

Wood SA, Crerar DA, Borcsik MP (1987) Solubility of the assemblage pyrite-pyrrhotite-magnetite-galena-gold-stibnite-bismuthinite-argentite-molybdenite in H_2O-NaCl-CO_2 solutions from 200°C to 350°C. Econ Geol 82:1864–1887

Wu SR (2008) Geological characteristics and genetic analysis of the Paiting gold deposit, Guizhou Province. Mineral Resour Geol 22: 55–61 **(in Chinese with English abstract)**

Xia Y, Zhang Y, Su WC, Tao Y, Zhang XC, Liu JZ, Deng YM (2009) Metallogenic model and prognosis of the Shuiyindong super-large stratabound Carlin-type gold deposit, Southwestern Guizhou Province, China. Acta Geol Sin 83:1473–1482 **(in Chinese with English abstract)**

Zhang XC, Spiro B, Halls C, Stanley C, Yang KY (2003) Sediment-hosted disseminated gold deposits in southwest Guizhou, PRC: their geological setting and origin in relation to mineralogical, fluid inclusion, and stable-isotope characteristics. Int Gel Rev 45:407–470

Zhuang HP, Lu JL, Fu JM, Liu DH (1998) Two paragenetic types of the Carlin-type gold deposits in southwestern Guizhou Province. Chin Sci Bull 43:977–982 **(in Chinese with English abstract)**